Table 3
Basic Information of Light Curves

	Spectroscopy			Continuum			Hβ	
Name	Season	Duration	Epochs	Cadence	F_{var} (days)	Flux density (%)	F_{var}	Flux (%)
(1)	(2)	(3)	(4)	(5)	(6)	(7)	(8)	(9)
PG 0007+106	All	2017.10–2021.01	132	8.9	10.4 ± 0.7	0.95 ± 0.10	11.3 ± 0.7	1.51 ± 0.17
	1	2017.10–2018.01	23	4.3	7.5 ± 1.2	1.08 ± 0.08	5.5 ± 0.9	1.61 ± 0.09
	2	2018.08–2019.02	47	3.4	3.8 ± 0.5	0.95 ± 0.04	7.8 ± 0.9	1.64 ± 0.13
	3	2019.06–2020.02	35	6.5	11.3 ± 1.4	0.93 ± 0.11	8.2 ± 1.1	1.40 ± 0.12
	4	2020.08–2021.01	27	5.1	4.8 ± 0.9	0.86 ± 0.05	7.3 ± 1.1	1.35 ± 0.10
PG 0049+171	All	2017.10–2021.02	160	7.5	13.4 ± 0.8	1.77 ± 0.24	5.9 ± 0.4	1.88 ± 0.12
	1	2017.10–2018.02	28	4.5	6.4 ± 0.9	1.89 ± 0.13	7.2 ± 1.1	2.01 ± 0.15
	2	2018.08–2019.02	48	3.7	5.4 ± 0.6	1.50 ± 0.08	2.2 ± 0.4	1.78 ± 0.05
	3	2019.06–2020.02	44	5.5	8.9 ± 1.0	2.00 ± 0.18	3.3 ± 0.5	1.92 ± 0.08
	4	2020.08–2021.02	40	4.3	6.5 ± 0.8	1.74 ± 0.12	2.9 ± 0.5	1.85 ± 0.07
PG 0923+129	All	2020.10–2021.05	41	5.0	6.3 ± 0.8	4.41 ± 0.30	8.5 ± 1.0	1.90 ± 0.17
PG 0947+396	All	2017.10–2021.05	83	15.7	6.9 ± 0.6	0.57 ± 0.04	6.3 ± 0.6	0.49 ± 0.03
	1	2017.10–2018.05	26	7.8	7.5 ± 1.3	0.55 ± 0.05	9.7 ± 1.4	0.48 ± 0.05
	2	2018.11–2019.06	22	10.2	8.2 ± 1.3	0.57 ± 0.05	3.3 ± 0.8	0.50 ± 0.02
	3	2020.02–2020.05	16	7.2	1.1 ± 0.7	0.60 ± 0.01	4.3 ± 0.9	0.50 ± 0.02
	4	2020.11–2021.05	19	10.4	4.6 ± 1.0	0.56 ± 0.03	3.2 ± 0.8	0.48 ± 0.02
PG 1001+054	All	2017.10–2021.05	102	12.8	7.8 ± 0.6	0.81 ± 0.06	5.5 ± 0.4	0.81 ± 0.05
	1	2017.10–2018.04	31	5.8	2.6 ± 0.4	0.80 ± 0.02	2.4 ± 0.4	0.83 ± 0.02
	2	2018.10–2019.06	34	6.6	2.8 ± 0.4	0.75 ± 0.02	1.8 ± 0.5	0.77 ± 0.02
	3	2019.11–2020.05	23	8.1	4.3 ± 0.7	0.90 ± 0.04	3.5 ± 0.6	0.85 ± 0.03
	4	2020.11–2021.05	14	14.1	3.5 ± 0.9	0.85 ± 0.03	5.9 ± 1.4	0.86 ± 0.06
PG 1048+342	All	2017.11–2021.05	87	14.4	11.1 ± 0.9	0.58 ± 0.07	8.0 ± 0.7	0.52 ± 0.04
	1	2017.11–2018.05	23	7.3	5.8 ± 1.2	0.49 ± 0.03	3.4 ± 0.7	0.46 ± 0.02
	2	2018.11–2019.06	36	6.2	3.5 ± 0.6	0.63 ± 0.03	2.6 ± 0.6	0.56 ± 0.02
	3	2019.11–2020.04	13	11.9	2.3 ± 1.8	0.60 ± 0.03	1.3 ± 1.2	0.54 ± 0.02
	4	2020.12–2021.05	15	10.2	6.5 ± 1.5	0.55 ± 0.04	2.1 ± 0.8	0.54 ± 0.02
PG 1100+772	All	2018.11–2021.04	42	20.9	8.9 ± 1.0	1.37 ± 0.13	1.6 ± 0.5	2.32 ± 0.06
PG 1202+281	All	2016.12–2021.04	101	15.5	9.2 ± 0.7	0.58 ± 0.05	7.4 ± 0.6	0.37 ± 0.03
	1	2016.12–2017.05	26	5.7	6.4 ± 1.0	0.59 ± 0.04	3.7 ± 0.7	0.34 ± 0.02
	2	2018.01–2018.05	22	5.5	5.4 ± 0.9	0.60 ± 0.03	1.0 ± 0.8	0.35 ± 0.01
	3	2018.12–2019.07	27	7.8	10.1 ± 1.4	0.58 ± 0.06	2.6 ± 0.6	0.40 ± 0.01
	4	2020.01–2020.05	21	6.4	6.2 ± 1.0	0.54 ± 0.03	4.4 ± 0.8	0.36 ± 0.02
	5	2020.12–2021.04	5	23.8	6.3 ± 2.1	0.47 ± 0.03	5.3 ± 1.8	0.36 ± 0.02
PG 1211+143	All	2016.12–2017.07	52	4.2	12.1 ± 1.3	4.66 ± 0.58	10.3 ± 1.1	4.61 ± 0.50
PG 1310-108	All	2021.01–2021.05	17	7.7	3.3 ± 0.9	1.76 ± 0.08	3.3 ± 0.7	1.14 ± 0.04
PG 1351+640	All	2016.12–2021.02	109	13.8	14.1 ± 1.0	3.63 ± 0.51	4.7 ± 0.4	1.22 ± 0.06
PG 1351+695	All	2019.06–2021.04	108	6.2	12.2 ± 0.9	3.80 ± 0.47	26.9 ± 1.9	1.75 ± 0.48
PG 1501+106	All	2017.02–2020.06	136	8.9	13.2 ± 0.8	5.18 ± 0.69	7.6 ± 0.5	3.61 ± 0.28
	1	2017.02–2017.05	17	6.1	8.6 ± 1.6	6.06 ± 0.53	6.9 ± 1.2	3.67 ± 0.26
	2	2018.01–2018.05	28	4.3	2.9 ± 0.5	5.64 ± 0.18	2.7 ± 0.5	3.69 ± 0.11
	3	2019.02–2019.10	57	4.3	9.0 ± 0.9	5.20 ± 0.47	10.0 ± 1.0	3.64 ± 0.37
	4	2020.01–2020.06	34	3.9	7.2 ± 0.9	4.34 ± 0.32	4.1 ± 0.5	3.47 ± 0.15
PG 1534+580	All	2020.02–2021.05	83	5.5	5.8 ± 0.5	3.90 ± 0.24	6.0 ± 0.6	1.85 ± 0.12
PG 1613+658	All	2016.12–2021.04	200	7.9	11.9 ± 0.6	2.62 ± 0.32	5.1 ± 0.3	3.55 ± 0.20
	1	2016.12–2018.05	55	9.2	12.2 ± 1.2	2.84 ± 0.35	3.7 ± 0.5	3.78 ± 0.17
	2	2018.12–2021.04	145	6.0	10.0 ± 0.6	2.53 ± 0.26	3.0 ± 0.3	3.46 ± 0.13

Note. Column 1 is the name of object. Column 2 is the season for the measurement. Columns 3–5 are the duration, epoch, and cadence of the spectroscopy. Columns 6–7 are the variation amplitude and mean flux for the continuum light curve. The uncertainty range of the mean flux is the standard deviation of the light curve. The unit of the mean flux is 10^{-15} erg s^{-1} cm^{-2} Å^{-1}. Columns 8–9 are the variation amplitude and mean flux for the Hβ light curve. The unit of the mean flux is 10^{-13} erg s^{-1} cm^{-2}.

uncertainties generated from MICA are shown in Figures 2–16. The time lags and their uncertainties are given in Table 6. For the light curves with clear variations and statistically significant time delays (e.g., Season 4 of PG 0049+171; Season 2 of PG 0947+396, PG 1310−108), the measurements of the three methods are generally consistent with each other. The pairwise comparison between the lag measurements of the methods are demonstrated in Figure 17. The results from ICCF and MICA have the best consistency, while the χ^2 method generally gives larger scatter compared to the other two methods. Considering that MICA takes advantage of a damped random walk model (Li et al. 2016) and can give better constraints to the light-curve reconstruction by incorporating the continuum and Hβ variations, in particular across larger gaps, we adopted the time lags from MICA for the BH mass measurements in the following Section 3.6.

Table 4
Systematic Errors of Light Curves

Target	Duration	σ_{sys} (conti)	σ_{sys} (Hβ)
PG 0007+106	2017.10–2018.01	0.019	0.026
PG 0007+106	2018.08–2019.02	0.015	0.031
PG 0007+106	2019.06–2020.02	0.022	0.034
PG 0007+106	2020.08–2021.01	0.022	0.026
PG 0049+171	2017.10–2018.02	0.037	0.042
PG 0049+171	2018.08–2019.02	0.014	0.028
PG 0049+171	2019.06–2020.02	0.030	0.043
PG 0049+171	2020.08–2021.02	0.021	0.038
PG 0923+129	2020.10–2021.05	0.000	0.000
PG 0947+396	2017.10–2018.05	0.017	0.009
PG 0947+396	2018.11–2019.06	0.003	0.000
PG 0947+396	2020.02–2020.05	0.000	0.000
PG 0947+396	2020.11–2021.05	0.009	0.000
PG 1001+054	2017.10–2018.04	0.010	0.011
PG 1001+054	2018.10–2019.06	0.007	0.013
PG 1001+054	2019.11–2020.05	0.009	0.013
PG 1001+054	2020.11–2021.05	0.011	0.020
PG 1048+342	2017.11–2018.05	0.017	0.007
PG 1048+342	2018.11–2019.06	0.005	0.007
PG 1048+342	2019.11–2020.04	0.022	0.010
PG 1048+342	2020.12–2021.05	0.013	0.004
PG 1100+772	2018.11–2019.09	0.000	0.000
PG 1100+772	2019.10–2020.05	0.000	0.000
PG 1100+772	2020.11–2021.04	0.017	0.000
PG 1202+281	2016.12–2017.05	0.014	0.007
PG 1202+281	2018.01–2018.05	0.012	0.006
PG 1202+281	2018.12–2019.07	0.009	0.007
PG 1202+281	2020.01–2020.05	0.008	0.006
PG 1202+281	2020.12–2021.04	0.007	0.004
PG 1211+143	2016.12–2017.07	0.148	0.146
PG 1310-108	2021.01–2021.05	0.038	0.000
PG 1351+640	2016.12–2017.05	0.000	0.020
PG 1351+640	2017.12–2018.05	0.020	0.021
PG 1351+640	2019.01–2019.11	0.049	0.021
PG 1351+640	2020.02–2020.05	0.002	0.025
PG 1351+640	2020.08–2021.02	0.036	0.030
PG 1351+695	2019.06–2020.05	0.061	0.036
PG 1351+695	2020.08–2021.04	0.108	0.136
PG 1501+106	2017.02–2017.05	0.098	0.043
PG 1501+106	2018.01–2018.05	0.056	0.048
PG 1501+106	2019.02–2019.10	0.041	0.046
PG 1501+106	2020.01–2020.06	0.000	0.019
PG 1534+580	2020.02–2020.05	0.037	0.029
PG 1534+580	2020.08–2021.05	0.070	0.051
PG 1613+658	2016.12–2017.05	0.022	0.083
PG 1613+658	2018.01–2018.05	0.000	0.000
PG 1613+658	2018.12–2020.05	0.027	0.058
PG 1613+658	2020.08–2021.04	0.027	0.048

Note. These are the systematic errors of the spectroscopy data in separate seasons. The systematic error of "0.000" means that it can be ignored. For PG 1100+772, PG 1351+640, PG 1351+695, PG 1534+580, and PG 1613+658, we did not divide their light curves into different seasons according to their gaps in the campaign because of the long variation timescales (see details in Section 2.2). However, their systematic uncertainties for continuum and Hβ used in the time-series analysis in Section 3 are estimated in light of the gaps in the campaign (if necessary). The unit for continuum systematic errors is 10^{-15} erg s^{-1} cm^{-2} Å^{-1}. The unit for Hβ systematic errors is 10^{-13} erg s^{-1} cm^{-2}.

3.6. Black Hole Masses

Given the time lag and the line width measurements, the BH masses $M_\bullet$ can be determined by the formula

$$M_\bullet = f_{\rm BLR}\frac{R_{\rm BLR}V^2}{G}, \quad (9)$$

where $R_{\rm BLR} = c\tau_{\rm BLR}$ is the responsivity-weighted radius of the BLR, $\tau_{\rm BLR}$ is the time lag, c is the speed of light, V is $\sigma_{\rm H\beta}$ or FWHM of the Hβ line from the mean or rms spectra, G is the gravitational constant, and $f_{\rm BLR}$ is a scaling factor.

The average value of $f_{\rm BLR}$ for AGNs as a sample can be determined by calibration against the $M_\bullet$–σ_* or $M_\bullet$–M_* relationships of inactive galaxies (e.g., Onken et al. 2004; Woo et al. 2010, 2015; Ho & Kim 2014), where σ_* and M_* are the stellar velocity dispersion and stellar mass of the galactic bulge. However, the specific values of $f_{\rm BLR}$ in individual objects are likely to have a significant scatter around the average (e.g., Pancoast et al. 2014; Grier et al. 2017; Li et al. 2018; Williams et al. 2018). Here we adopt the calibrated average $f_{\rm BLR}$ from Woo et al. (2015; 1.12 for FWHM and 4.47 for $\sigma_{\rm H\beta}$) in our $M_\bullet$ calculations, as we did for Papers I and II.

It has been suggested that the line widths in the rms spectra and time lags are more consistent with the virial relationship ($\tau \propto V^{-2}$) than the mean spectra (e.g., Peterson et al. 2004; Dalla Bontà et al. 2020). Therefore, we calculated the BH masses using the line widths from the rms spectra. But for completeness, we provided the "virial products (VP)" measured from the FWHM of the mean spectra ($R_{\rm H\beta}V^2_{\rm FWHM}/G$). We divided the light curves of the objects according to their seasonal gaps and measured the time lags for different seasons (Section 2.2) as well as for combined seasons. Table 7 gives the corresponding VP measured from the mean spectra, as well as BH masses ($f_{\rm BLR}R_{\rm BLR}V^2/G$) measured from the FWHM and $\sigma_{\rm H\beta}$ of the rms spectra; seasons with very poor lag measurements are ignored in the mass determinations. For completeness, the monochromatic luminosity at 5100 Å is available in Table 6. It should be noted that we have corrected for the Galactic extinction, but host-galaxy contamination is present in these measurements. We will investigate the location of our targets on the radius–luminosity plane (e.g., Kaspi et al. 2000; Bentz et al. 2013; Du & Wang 2019) in a future paper. The cosmological parameters used to calculate the luminosity are $H_0 = 67$ km s^{-1} Mpc^{-1}, $\Omega_M = 0.32$, $\Omega_\Lambda = 0.68$ (Planck Collaboration et al. 2014, 2020).

The time lags can vary over time, for instance if there are strong luminosity changes. In principle, it should not make a difference to the measurement of BH mass if we use the time lag from the light curves of any individual season or from the entire campaign, as the BH mass cannot change on short timescales. In practice, some seasons have stronger variations and better sampling than others. However, if the BLR kinematics is complex or variable, the BH masses measured from individual seasons or the whole

Table 5
Light Curves

Target	Telescope	Data	JD	Flux
PG 0007+106	WIRO	Conti	1046.674	0.982 ± 0.004
PG 0007+106	WIRO	Hβ	1046.674	1.501 ± 0.007
PG 0007+106	WIRO	Conti	1049.699	0.963 ± 0.004
PG 0007+106	WIRO	Hβ	1049.699	1.519 ± 0.006
PG 0007+106	WIRO	Conti	1050.721	0.985 ± 0.005
PG 0007+106	WIRO	Hβ	1050.721	1.473 ± 0.008

Note. The uncertainty does not include the systematic errors measured from median-filter method (see Section 3.2). The Julian dates are from 2,457,000. The units for continuum and Hβ are 10^{-15} erg s^{-1} cm^{-2} Å^{-1} and 10^{-13} erg s^{-1} cm^{-2}, respectively.

(This table is available in its entirety in machine-readable form.)

Table 6
Line Widths, Time Lags in the Rest Frame, and 5100 Å Luminosity

Target	Mean Spectra		rms		ICCF		MICA	χ^2		λL_λ(5100 Å)
	Season	FWHM (km s^{-1})	$\sigma_{\rm line}$ (km s^{-1})	FWHM (km s^{-1})	$\sigma_{\rm line}$ (km s^{-1})	$\tau_{\rm cent}$ (days)	$\tau_{\rm peak}$ (days)	$\tau_{\rm cent}$ (days)	$\tau_{\rm peak}$ (days)	($\times 10^{44}$ erg s^{-1})
PG 0007+106	All	5301^{+33}_{-28}	2424^{+39}_{-41}	4832^{+10}_{-11}	1766^{+11}_{-9}	$30.9^{+2.5}_{-2.4}$	$25.1^{+1.9}_{-4.4}$	$25.8^{+1.2}_{-1.1}$	$24.2^{+3.8}_{-3.2}$	1.61 ± 0.17
	1	5365^{+28}_{-28}	2524^{+43}_{-44}	5396^{+25}_{-24}	1895^{+21}_{-21}	$22.1^{+7.8}_{-5.7}$	$19.5^{+24.3}_{-4.0}$	$23.3^{+6.2}_{-4.0}$	$51.2^{+7.8}_{-32.9}$	1.84 ± 0.14
	2	5244^{+33}_{-30}	2347^{+34}_{-34}	4621^{+7}_{-6}	1881^{+13}_{-14}	$34.7^{+4.0}_{-4.3}$	$32.0^{+5.6}_{-7.6}$	$19.7^{+9.3}_{-13.7}$	$15.0^{+4.4}_{-2.7}$	1.62 ± 0.07
	3	5433^{+44}_{-29}	2365^{+41}_{-37}	4471^{+29}_{-29}	1750^{+24}_{-24}	$15.6^{+15.4}_{-11.1}$	$14.4^{+4.5}_{-6.0}$	$14.3^{+2.5}_{-2.6}$	$4.6^{+19.3}_{-150.2}$	1.58 ± 0.18
	4	5176^{+37}_{-24}	2558^{+56}_{-53}	4686^{+9}_{-10}	1558^{+14}_{-12}	$25.1^{+10.4}_{-6.7}$	$20.7^{+6.9}_{-3.8}$	$20.8^{+2.1}_{-2.0}$	$98.2^{+9.8}_{-12.9}$	1.45 ± 0.08
PG 0049+171	All	4262^{+411}_{-38}	2272^{+38}_{-32}	2873^{+7}_{-4}	1193^{+13}_{-13}	$34.7^{+3.8}_{-4.5}$	$28.1^{+11.4}_{-5.5}$	$39.5^{+3.3}_{-2.6}$	$84.9^{+43.7}_{-31.4}$	1.27 ± 0.17
	1	4131^{+394}_{-48}	2005^{+45}_{-46}	2804^{+9}_{-17}	1109^{+17}_{-21}	$51.2^{+3.7}_{-3.8}$	$54.2^{+5.2}_{-9.9}$	$41.8^{+7.2}_{-6.3}$	$31.8^{+20.9}_{-20.6}$	1.36 ± 0.09
	2	4426^{+399}_{-95}	2309^{+37}_{-42}	2919^{+13}_{-8}	1370^{+14}_{-13}	$23.7^{+14.0}_{-4.4}$	$22.2^{+9.4}_{-4.6}$	$30.9^{+3.7}_{-7.6}$	$27.1^{+36.8}_{-9.5}$	1.07 ± 0.06
	3	4296^{+311}_{-47}	2333^{+36}_{-32}	1896^{+9}_{-7}	988^{+21}_{-19}	$33.0^{+6.7}_{-9.3}$	$34.6^{+5.1}_{-11.4}$	$46.3^{+64.3}_{-8.6}$	$28.2^{+13.3}_{-10.3}$	1.44 ± 0.13
	4	4222^{+478}_{-42}	2327^{+52}_{-36}	3425^{+12}_{-13}	1223^{+19}_{-23}	$20.4^{+4.0}_{-3.4}$	$20.6^{+4.4}_{-3.6}$	$22.6^{+2.7}_{-2.2}$	$20.3^{+7.7}_{-5.2}$	1.25 ± 0.08
PG 0923+129	All	2461^{+34}_{-34}	1711^{+51}_{-48}	2138^{+17}_{-13}	1215^{+20}_{-19}	$4.6^{+3.4}_{-4.8}$	$5.5^{+1.6}_{-3.7}$	$6.2^{+3.2}_{-1.8}$	$5.0^{+4.5}_{-90.5}$	0.56 ± 0.04
PG 0947+396	All	5440^{+24}_{-76}	2872^{+33}_{-27}	3292^{+28}_{-33}	2021^{+27}_{-32}	$34.4^{+4.5}_{-4.9}$	$36.3^{+8.4}_{-8.9}$	$39.5^{+3.8}_{-1.7}$	$41.4^{+6.8}_{-10.8}$	5.85 ± 0.43
	1	5222^{+44}_{-24}	2797^{+36}_{-33}	3757^{+28}_{-37}	1653^{+26}_{-29}	$18.4^{+6.0}_{-6.8}$	$17.4^{+15.5}_{-14.1}$	$15.9^{+7.0}_{-7.8}$	$24.8^{+44.7}_{-18.9}$	5.68 ± 0.47
	2	5156^{+68}_{-24}	2816^{+33}_{-27}	5002^{+15}_{-16}	1673^{+12}_{-14}	$38.5^{+5.6}_{-5.8}$	$41.1^{+6.2}_{-8.0}$	$41.8^{+1.3}_{-1.1}$	$44.8^{+8.1}_{-7.5}$	5.89 ± 0.51
	3	5590^{+24}_{-93}	2906^{+20}_{-22}	4216^{+21}_{-19}	1470^{+15}_{-17}	$57.1^{+10.7}_{-9.5}$	$48.5^{+17.0}_{-20.4}$	$32.6^{+16.1}_{-18.2}$	$34.9^{+59.4}_{-16.6}$	6.17 ± 0.13
	4	5783^{+97}_{-34}	2984^{+28}_{-22}	6181^{+46}_{-28}	1861^{+35}_{-32}	$46.9^{+6.0}_{-11.2}$	$48.9^{+5.5}_{-18.0}$	$29.4^{+10.0}_{-4.0}$	$48.2^{+12.4}_{-18.1}$	5.78 ± 0.31
PG 1001+054	All	1688^{+21}_{-21}	1325^{+18}_{-18}	1933^{+31}_{-20}	1370^{+44}_{-62}	$99.4^{+15.8}_{-27.2}$	$68.0^{+11.2}_{-16.0}$	$65.5^{+5.6}_{-3.9}$	$63.3^{+17.4}_{-11.2}$	4.46 ± 0.35
	3	1666^{+11}_{-11}	1318^{+11}_{-11}	917^{+60}_{-50}	840^{+134}_{-185}	$57.6^{+18.9}_{-13.5}$	$63.0^{+22.6}_{-28.1}$	$64.7^{+11.2}_{-6.9}$	$117.0^{+11.5}_{-62.5}$	4.93 ± 0.22
PG 1048+342	All	2905^{+27}_{-59}	1797^{+16}_{-16}	2147^{+8}_{-7}	1175^{+16}_{-14}	$24.8^{+10.4}_{-8.7}$	$32.6^{+13.3}_{-32.6}$	$36.8^{+2.4}_{-3.4}$	$31.8^{+77.2}_{-35.5}$	3.52 ± 0.41
	1	3004^{+34}_{-45}	1840^{+16}_{-14}	3043^{+33}_{-34}	1449^{+36}_{-31}	$26.2^{+8.6}_{-8.2}$	$25.5^{+13.7}_{-8.2}$	$28.0^{+5.6}_{-4.8}$	$33.6^{+11.1}_{-11.9}$	3.02 ± 0.21
PG 1100+772	All	5733^{+32}_{-21}	3449^{+31}_{-30}	11229^{+29}_{-23}	4002^{+87}_{-110}	$44.9^{+30.5}_{-30.8}$	$37.4^{+45.3}_{-27.5}$	$55.9^{+3.0}_{-1.4}$	$48.6^{+46.6}_{-120.9}$	41.95 ± 3.85
PG 1202+281	All	5199^{+24}_{-22}	2035^{+5}_{-4}	4255^{+23}_{-17}	1301^{+18}_{-24}	$98.5^{+28.2}_{-30.1}$	$66.4^{+65.7}_{-13.4}$	$66.3^{+2.3}_{-1.9}$	$116.3^{+39.4}_{-31.4}$	3.42 ± 0.32
	1	4891^{+19}_{-19}	3412^{+12}_{-12}	3825^{+38}_{-70}	1597^{+17}_{-19}	$50.0^{+6.6}_{-4.6}$	$50.4^{+7.9}_{-5.1}$	$48.7^{+3.5}_{-3.9}$	$74.4^{+8.8}_{-27.8}$	3.52 ± 0.24
	3	4863^{+22}_{-16}	3260^{+20}_{-17}	3814^{+399}_{-747}	1540^{+53}_{-63}	$71.6^{+15.6}_{-9.5}$	$68.7^{+36.6}_{-7.1}$	$69.5^{+4.8}_{-4.4}$	$133.0^{+28.2}_{-68.8}$	3.45 ± 0.36
	4	4949^{+16}_{-16}	3738^{+25}_{-24}	3658^{+26}_{-29}	1428^{+29}_{-33}	$53.3^{+10.9}_{-8.5}$	$46.5^{+22.4}_{-11.1}$	$63.3^{+13.3}_{-12.9}$	$79.4^{+37.4}_{-22.1}$	3.22 ± 0.21
PG 1211+143	All	1918^{+95}_{-95}	1499^{+49}_{-49}	1358^{+14}_{-11}	697^{+18}_{-19}	$33.0^{+5.6}_{-5.5}$	$47.5^{+10.8}_{-8.9}$	$53.0^{+5.1}_{-5.8}$	$43.7^{+18.2}_{-17.5}$	4.94 ± 0.56
PG 1310-108	All	3613^{+812}_{-781}	1978^{+87}_{-65}	2425^{+15}_{-19}	1092^{+36}_{-54}	$13.2^{+3.8}_{-2.8}$	$12.5^{+3.6}_{-2.1}$	$12.8^{+1.7}_{-1.7}$	$12.6^{+6.8}_{-3.5}$	0.33 ± 0.01
PG 1351+640	All	7625^{+95}_{-81}	3114^{+65}_{-50}	2154^{+18}_{-13}	1527^{+23}_{-21}	$68.6^{+20.4}_{-20.7}$	$61.6^{+81.3}_{-27.6}$	$74.8^{+2.3}_{-2.3}$	$-31.5^{+77.8}_{-37.2}$	4.87 ± 0.69
PG 1351+695	All	5297^{+10}_{-10}	1871^{+6}_{-6}	4478^{+3}_{-3}	1583^{+12}_{-10}	$18.6^{+2.3}_{-2.0}$	$16.7^{+4.1}_{-1.9}$	$19.9^{+1.0}_{-1.0}$	$11.7^{+6.0}_{-5.3}$	0.50 ± 0.06
PG 1501+106	All	5006^{+50}_{-32}	2490^{+47}_{-47}	4152^{+8}_{-5}	1986^{+14}_{-17}	$26.0^{+2.0}_{-2.2}$	$24.0^{+4.6}_{-6.1}$	$22.0^{+0.5}_{-0.4}$	$113.7^{+10.7}_{-66.2}$	1.03 ± 0.14
	1	5081^{+26}_{-44}	2528^{+50}_{-43}	3855^{+13}_{-14}	2291^{+18}_{-19}	$24.1^{+10.8}_{-8.8}$	$6.1^{+17.9}_{-3.2}$	$5.0^{+1.3}_{-1.4}$	$117.0^{+7.5}_{-43.7}$	1.20 ± 0.11
	3	5002^{+34}_{-53}	2454^{+47}_{-44}	4141^{+5}_{-5}	1384^{+10}_{-12}	$24.8^{+1.6}_{-1.4}$	$24.9^{+1.8}_{-1.6}$	$42.9^{+9.9}_{-4.7}$	$25.9^{+3.0}_{-1.8}$	1.03 ± 0.09
	4	4718^{+43}_{-41}	2378^{+56}_{-45}	2945^{+17}_{-18}	1156^{+14}_{-14}	$32.2^{+3.6}_{-4.0}$	$24.8^{+16.8}_{-7.5}$	$43.7^{+3.7}_{-2.7}$	$108.8^{+5.5}_{-23.0}$	0.86 ± 0.06
PG 1534+580	All	4217^{+751}_{-155}	3180^{+84}_{-47}	2362^{+11}_{-7}	1142^{+20}_{-20}	$26.0^{+5.7}_{-8.6}$	$35.5^{+3.5}_{-21.6}$	$25.4^{+2.0}_{-1.4}$	$28.2^{+9.3}_{-14.0}$	0.48 ± 0.03
PG 1613+658	All	$10{,}269^{+773}_{-167}$	3927^{+13}_{-16}	6762^{+9}_{-10}	3504^{+13}_{-14}	$51.2^{+5.2}_{-6.0}$	$55.8^{+10.5}_{-22.9}$	$52.4^{+3.4}_{-2.8}$	$27.6^{+13.0}_{-13.0}$	8.62 ± 1.04
	1	9866^{+118}_{-132}	3907^{+14}_{-13}	12817^{+36}_{-30}	4654^{+18}_{-16}	$49.7^{+9.2}_{-10.2}$	$42.9^{+31.1}_{-10.9}$	$79.3^{+5.9}_{-2.8}$	$91.8^{+10.0}_{-32.7}$	9.36 ± 1.16
	2	$10{,}998^{+193}_{-221}$	3926^{+13}_{-14}	11469^{+25}_{-48}	4196^{+20}_{-29}	$46.3^{+7.3}_{-7.3}$	$45.9^{+11.4}_{-13.3}$	$48.3^{+5.0}_{-3.8}$	$-191.1^{+223.2}_{-11.0}$	8.34 ± 0.85

Note. The line widths of the rms spectra of PG 0049+171, PG 0947+396, PG 1202+281, PG 1351+640, and PG 1501+106 are measured from their continuum-cleaned rms spectra (See Section 3.1). The broadening caused by the instrument and seeing has been corrected. For 5100 Å luminosity, the galactic extinction (Schlafly & Finkbeiner 2011) is corrected, but the host-galaxy contamination is not removed. The time lags in the table are in the rest frame.

light curves can perhaps differ. BLR dynamical modeling (e.g., Pancoast et al. 2011, 2014; Li et al. 2013, 2018) can, in principle, give more reliable BH mass measurements if the BLRs deviate from Keplerian/virialized motion, but this discussion stretches beyond the scope of the current paper. The best data sets here may be good enough to allow dynamical modeling, which we shall investigate in future work.

For each object, we list the measurements from the whole light curve and from all of the seasons (except for the very poor ones) in Table 7 and mark the preferred values with a "✓" (the ones calculated from $\sigma_{\rm H\beta}$ in the rms spectra). We prefer to adopt the results with the smallest measurement uncertainties. They are usually the values measured from the whole light curves, except for those objects for which the lag measurements of individual seasons have comparable or significantly smaller measurement uncertainties.

3.7. Velocity-resolved Results

To investigate the BLR geometry and kinematics and their potential changes over time for the present sample, we calculated velocity-resolved lags (e.g., Bentz et al. 2009; Denney et al. 2010; Grier et al. 2013; Du et al. 2016a; Hu et al. 2020a) as a first step. We divided the emission lines into several bins, determined by the flux ranges in the rms spectra, and measured their time lags with respect to the continuum using ICCF. The lags as functions of velocity are shown in Figure 18. Similar to the BH mass measurements in Section 3.6, because of the limitations of variation amplitudes

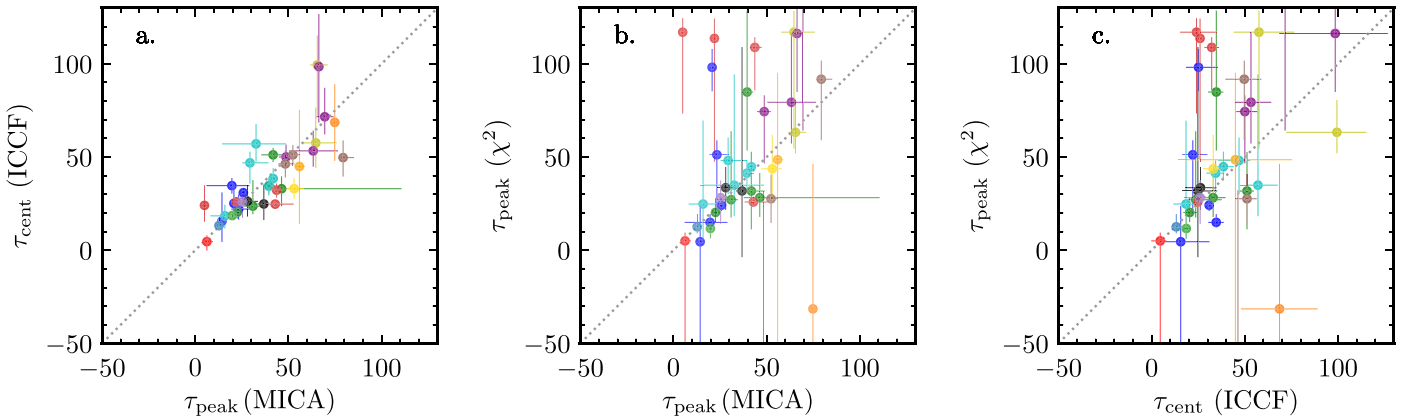

Figure 17. Pairwise correlations between the measurements from ICCF, χ^2, and MICA. The points in the same color are the time lags of different seasons (and the entire light curve) for individual objects.

and S/N ratios, we cannot obtain the velocity-resolved lag measurements for all of the objects for all individual seasons. We did not calculate the velocity-resolved lags for the seasons with poor data or no clear variations. For the objects with very weak Hβ signals in the rms spectra (see Section 3.1), we instead determined their velocity bins using the mean spectra. It has been demonstrated that using mean or rms spectra to determine the velocity bins does not usually change the results significantly (see more details in Paper I).

4. Discussion

One of the primary goals of the MAHA project is to investigate the BLR geometry and kinematics as well as their potential evolution in AGN BLRs with asymmetric Hβ lines, which requires both long-term monitoring and high cadence. More than half of the present sample (nine objects) have been monitored for 4–5 yr with cadences of ∼3–8 days. Among them, six objects (see Table 7) show clear variations in more than one season and can be used to investigate the potential evolution in their BLR responses. Here we discuss the measurements of the individual objects and compare them with the previous results in the literature.

4.1. Notes for Individual Objects

PG 0007+106 (Mrk 1501, III Zw 2): It is a radio-loud AGN and showed a 5.1 yr quasiperiodicity in its radio light curve, which can perhaps be explained by the helical motion of a jet (Teräsranta et al. 2005; Li et al. 2010). In our RM campaign, Hβ time lags of ∼14–25 days (MICA) were measured for different seasons. From the four seasons and the combined light curve, BH mass measurements of 4–7 $\times$ $10^7 M_\odot$ were obtained using the line dispersion for the velocity measurement ($7.03^{+0.34}_{-0.31}$ $\times$ $10^7 M_\odot$ is preferred). The previous RM campaign of this object (Grier et al. 2012) gave a time lag of $15.5^{+2.2}_{-1.8}$ days and a BH mass of $\log(M_\bullet/M_\odot) = 7.9^{+0.2}_{-0.2}$ was measured from BLR dynamical modeling (Grier et al. 2017). Our BH mass is in excellent agreement with that from Grier et al. (2017). In all of the four seasons, the velocity-resolved lags in Figure 18 show longer lags at small velocities and shorter lags at high velocities, which indicates that its BLR is dominated by virialized motions or a Keplerian disk (the data quality in Seasons 1 and 4 is relatively poorer). In Seasons 2 and 3, the velocities corresponding to the blue wing of the line have slightly longer lags than the red wing, implying a potential contribution of inflowing velocity besides the Keplerian/virialized motion in its BLR. Similarly, the BLR modeling in Grier et al. (2017) suggested that its BLR kinematics is a combination of near-circular elliptical and inflowing orbits. However, the velocity-resolved lags in Grier et al. (2013) showed a stronger inflowing signature. In our campaign, the Hβ profile is almost the same as that in Grier et al. (2012) and also similar to those seen in much earlier single-epoch spectra (De Robertis 1985; Boroson & Green 1992; Marziani et al. 2003a). Note that the excess red emission in the Hβ profile for this object is not well characterized by the De Robertis asymmetry parameter A. The A parameter measures the blue or red extension of line wing. The red wing of the Hβ in PG 0007+106 does not extend too much with respect to its line core. Instead the flux excess can be quantified by a systematic velocity shift (e.g., "Hβ shift" in Table 2 of Boroson & Green 1992). The relation between the BLR kinematics and emission-line profiles (including the velocity shift) will be discussed in detail in a forthcoming paper.

PG 0049+171 (Mrk 1148): The profile of its broad Hβ is slightly red asymmetric and showed no significant change during our campaign. Its profile remains similar to that in De Robertis (1985) and Boroson & Green (1992). The Hβ response in Season 4 is the best among the seasons. It gives a BH mass of $2.95^{+0.37}_{-0.31}$ $\times$ $10^7 M_\odot$. Considering that the line signal in the rms spectrum of Season 4 is not very significant (it is better in the continuum-cleaned rms spectrum), we prefer to use the mean spectrum to determine the velocity bins in the velocity-resolved analysis. In the velocity-resolved analysis, the plateau of the Hβ light curve at the end of Season 1 is too short to give a good constraint in some of the velocity bins; thus the lags at different velocities in Season 1 are not very well resolved. The velocity-resolved lags for the other seasons (Seasons 2, 3, 4) are almost the same and show longer lags in low-velocity bins and shorter lags at high velocities. Similar to PG 0007+106, which is the signature of a Keplerian disk or virialized motion. Moreover, compared to Season 3, the velocity-resolved lags in Seasons 2 and 4 look more symmetric. The lags for the blue wing for Seasons 3 are shorter than those for its red wing, which indicates a potential contribution from outflow in this season. The differences between Seasons 2, 3, and 4 may imply that the response region of the BLR in PG 0049+171 is undergoing some minor changes.

Table 7
Virial Products and Masses of the Black Holes

Target	Season	VP (Mean)	BH mass (rms)		Note
		$R_{\rm H\beta}V^2_{\rm FWHM}/G$	$1.12 \times R_{\rm H\beta}V^2_{\rm FWHM}/G$	$4.47 \times R_{\rm H\beta}\sigma^2_{\rm line}/G$	
	($\times 10^7 M_\odot$)	($\times 10^7 M_\odot$)	($\times 10^7 M_\odot$)		
PG 0007+106	All	$14.16^{+0.68}_{-0.62}$	$13.18^{+0.61}_{-0.56}$	$7.03^{+0.34}_{-0.31}$	✓
	1	$13.10^{+3.50}_{-2.23}$	$14.84^{+3.97}_{-2.53}$	$7.31^{+1.96}_{-1.26}$	
	2	$10.56^{+5.02}_{-7.33}$	$9.18^{+4.37}_{-6.38}$	$6.07^{+2.89}_{-4.22}$	
	3	$8.27^{+1.45}_{-1.52}$	$6.27^{+1.10}_{-1.15}$	$3.84^{+0.68}_{-0.71}$	
	4	$10.86^{+1.11}_{-1.03}$	$9.97^{+1.01}_{-0.94}$	$4.40^{+0.45}_{-0.42}$	
PG 0049+171	All	$14.02^{+2.95}_{-0.94}$	$7.13^{+0.60}_{-0.46}$	$4.91^{+0.42}_{-0.34}$	
	1	$13.92^{+3.58}_{-2.13}$	$7.18^{+1.24}_{-1.09}$	$4.49^{+0.79}_{-0.70}$	
	2	$11.83^{+2.55}_{-2.94}$	$5.77^{+0.68}_{-1.41}$	$5.07^{+0.61}_{-1.25}$	
	3	$16.69^{+23.30}_{-3.11}$	$3.64^{+5.06}_{-0.67}$	$3.95^{+5.49}_{-0.75}$	
	4	$7.85^{+2.02}_{-0.78}$	$5.79^{+0.70}_{-0.57}$	$2.95^{+0.37}_{-0.31}$	✓
PG 0923+129	All	$0.74^{+0.38}_{-0.21}$	$0.62^{+0.32}_{-0.18}$	$0.81^{+0.42}_{-0.23}$	✓
PG 0947+396	All	$22.79^{+2.19}_{-1.18}$	$9.35^{+0.91}_{-0.45}$	$14.06^{+1.40}_{-0.76}$	
	1	$8.47^{+3.72}_{-4.13}$	$4.91^{+2.16}_{-2.40}$	$3.80^{+1.67}_{-1.86}$	
	2	$21.70^{+0.90}_{-0.63}$	$22.87^{+0.74}_{-0.65}$	$10.22^{+0.36}_{-0.33}$	✓
	3	$19.90^{+9.79}_{-11.13}$	$12.68^{+6.24}_{-7.08}$	$6.16^{+3.03}_{-3.44}$	
	4	$19.16^{+6.53}_{-2.64}$	$24.52^{+8.33}_{-3.37}$	$8.87^{+3.03}_{-1.26}$	
PG 1001+054	All	$3.65^{+0.32}_{-0.23}$	$5.35^{+0.49}_{-0.34}$	$10.73^{+1.15}_{-1.17}$	✓
	3	$3.50^{+0.61}_{-0.38}$	$1.19^{+0.26}_{-0.18}$	$3.99^{+1.45}_{-1.81}$	
PG 1048+342	All	$6.07^{+0.41}_{-0.61}$	$3.71^{+0.24}_{-0.34}$	$4.44^{+0.31}_{-0.42}$	✓
	1	$4.94^{+0.99}_{-0.86}$	$5.68^{+1.14}_{-0.98}$	$5.14^{+1.06}_{-0.90}$	
PG 1100+772	All	$35.86^{+1.99}_{-0.91}$	$154.05^{+8.39}_{-3.78}$	$78.13^{+5.44}_{-4.72}$	✓
PG 1202+281	All	$34.99^{+1.27}_{-1.02}$	$26.25^{+0.96}_{-0.76}$	$9.80^{+0.44}_{-0.46}$	✓
	1	$22.76^{+1.66}_{-1.81}$	$15.59^{+1.17}_{-1.36}$	$10.85^{+0.82}_{-0.90}$	
	3	$32.08^{+2.21}_{-2.05}$	$22.10^{+4.87}_{-8.77}$	$14.39^{+1.40}_{-1.50}$	
	4	$30.26^{+6.35}_{-6.18}$	$18.51^{+3.89}_{-3.79}$	$11.26^{+2.41}_{-2.36}$	
PG 1211+143	All	$3.81^{+0.53}_{-0.56}$	$2.14^{+0.21}_{-0.24}$	$2.25^{+0.25}_{-0.28}$	✓
PG 1310-108	All	$3.25^{+1.53}_{-1.47}$	$1.64^{+0.22}_{-0.22}$	$1.33^{+0.20}_{-0.22}$	✓
PG 1351+640	All	$84.95^{+3.38}_{-3.18}$	$7.60^{+0.27}_{-0.25}$	$15.24^{+0.66}_{-0.64}$	✓
PG 1351+695	All	$10.88^{+0.57}_{-0.55}$	$8.71^{+0.46}_{-0.44}$	$4.35^{+0.24}_{-0.23}$	✓
PG 1501+106	All	$10.76^{+0.32}_{-0.25}$	$8.29^{+0.19}_{-0.16}$	$7.57^{+0.20}_{-0.20}$	
	1	$2.51^{+0.66}_{-0.73}$	$1.61^{+0.42}_{-0.47}$	$2.28^{+0.60}_{-0.66}$	
	3	$20.95^{+4.84}_{-2.33}$	$16.08^{+3.71}_{-1.76}$	$7.17^{+1.66}_{-0.79}$	✓
	4	$18.97^{+1.65}_{-1.22}$	$8.28^{+0.71}_{-0.52}$	$5.09^{+0.45}_{-0.34}$	
PG 1534+580	All	$8.80^{+3.21}_{-0.82}$	$3.09^{+0.24}_{-0.18}$	$2.89^{+0.25}_{-0.19}$	✓
PG 1613+658	All	$107.82^{+17.70}_{-6.74}$	$52.36^{+3.42}_{-2.79}$	$56.13^{+3.69}_{-3.02}$	✓
	1	$150.70^{+11.72}_{-6.63}$	$284.85^{+21.14}_{-10.01}$	$149.95^{+11.16}_{-5.32}$	
	2	$114.07^{+12.36}_{-10.16}$	$138.95^{+14.25}_{-11.11}$	$74.24^{+7.64}_{-5.99}$	

Note. The VP are calculated from the FWHM of mean spectra. BH masses are estimated using the FWHM and the sigma of rms spectra. The propagation errors are from line widths and time lags, and the uncertainties of f factor is not considered here. The last column notes the data set we preferred for the BH mass measurement.

PG 0923+129 (Mrk 705, Ark 202): We have only data of one season for this object and they varied strongly only toward the end of our campaign. An Hβ time lag is reported here for the first time. The time lag measured from MICA is $6.2^{+3.2}_{-1.8}$ days and the corresponding preferred BH mass is $0.81^{+0.42}_{-0.23} \times 10^7 M_\odot$. The broad H$\beta$ profile is slightly red asymmetric, and neither the Fe II or [O III] lines are particularly strong. Its velocity-resolved lags are clearly longer at blue velocities and shorter at red velocities, which is the signature of inflow (see Figure 18).

PG 0947+396: Its Hβ profile shows a red asymmetry and has no obvious changes compared with previous spectra published by Boroson & Green (1992) and Shang et al. (2007). Time lags can be detected for each of its four seasons, although the uncertainties for the second season are the smallest because of its stronger continuum variation and clear Hβ response (See Section 3.1). The MICA measurement from the entire light curve is consistent with the single-season result from Season 2 ($39.5^{+3.8}_{-1.7}$ days versus $41.8^{+1.3}_{-1.1}$ days). The lag in Season 2 yields a preferred BH mass of $1.02^{+0.04}_{-0.03} \times 10^8 M_\odot$. Its velocity-resolved lags in Seasons 1, 3, and 4 are generally symmetric with longer lags at small velocities and shorter lags at high velocities, which is the signature of a Keplerian disk or virialized motion (similar to PG 0007+106 and PG 0049 +171). The lags at blue velocities are a little longer than those at red velocities in Seasons 1 and 3, while the opposite is the case in Season 4. While this effect is not very pronounced, it may imply weak contributions from inflow and outflow, respectively. It is a little strange that the lags at different velocities in Season 2 are not fully resolved, although the